A comparative Study of Low-Rank-plus-Sparse Matrix Decomposition and Machine Learning for Non-Destructive Air-Ultrasound Defect Detection

Manar Al-Askary*, Udaya S.K.P. Miriya Thanthrige*, Pierre Pfeffer†, Luis Wachter†, Giovanni Schober† and Aydin Sezgin*
*Institute of Digital Communication Systems, Ruhr University Bochum, Bochum, Germany
† SKZ - German Plastics Center, SKZ-KFE gGmbH, Würzburg, Germany
{manar.al-askary, udaya.miriyathanthrige, aydin.sezgin} @rub.de,
{p.pfeffer, l.wachter, g.schober} @skz.de

***Abstract*—Defect detection plays an important role in product quality assurance in many industrial applications. Air-coupled ultrasound defect detection setups have the advantage that they are non-destructive and do not contaminate the investigated materials. However, this approach comes with some challenges due to the weak signaling response of the defects. Thus, sophisticated signal separation methods are required. To address this challenge, low-rank-plus-sparse recovery (LRPSR) is proposed and compared with state-of-the-art machine learning (ML) methods. The results obtained show that the LRPSR method achieves comparable results in terms of detection rate to those achieved by ML. Yet, for a small training data set, the LRPSR approach outperforms the ML algorithms. The small training data set is important for detecting defects of different production lines without having a time-consuming training process. In addition, a lower standard deviation of the detection rate of the LRPSR method is observed, which shows its suitability for real-time processing.**

***Index Terms*—Non-destructive testing, air-coupled ultrasound, low-rank-plus-sparse recovery, machine learning, deep learning, gradient boosting trees, rpca**

I. Introduction

In the processing and production industry, the competition towards high quality outcomes at low costs has been increasing steadily. Special requirements are needed for a real-time testing technology during the producing process, which is important for quality control [1]. Thus, the measurement setup needs to be easy to use and has to have low maintenance costs and low system prices.

An efficient examination method is guaranteed by air-coupled ultrasound measurement setups. They satisfy the needed requirements during industrial processing but, in turn, lead to a new challenge. However, a significant challenge is the high reflection loss due to the impedance difference between air and most test materials. Besides, there are also strong refraction effects caused by the different sound velocities [2], [3]. As a remedy, special ultrasonic transducers use adaptation layers to reduce the impedance difference to air and thus reduce reflection losses. An ultrasonic measurement setup was used in related work in [4], where plastics samples were examined for defects. The examination revealed a detection rate of 83 %. Consequently, defect detection using the air-coupled ultrasound is a demanding task due to the signaling responses of the defects that are weaker than the signaling response of the sample. Thus, signal separation methods are required for defect detection. An interesting observation, which serves as the motivation for the proposed method, is that the number of defects in a defective sample is typically limited because the quality of the production is very high in general, and thus, defects occur very rarely. Further, the signaling response of the sample itself can be represented mathematically as a low-rank structure. Therefore, the overall signaling response of a sample with defects is a combination of low-rank and sparse components. Thus, in this work, low-rank-plus-sparse recovery (LRPSR) is proposed to separate the sample's signaling response and the defects. Here, our objective is to decompose the overall signaling response of a sample with defects as a low-rank matrix (sample) and a sparse matrix (defects). As one of the popular approaches of low-rank-plus-spares recovery, the robust principal component analysis (RPCA) [5] is utilized in this work.

In [6], surface defect detection based on RPCA and entity sparsity pursuit (ESP) was proposed, utilizing three real-world and one synthetic defect data sets for evaluation. Our approach is different from [6], as our focus on defect detection is based on an air-coupled ultrasound measurement system. Further, in this work, we examine the effect of reducing the training data size using the RPCA approach, and we compare the results with machine learning (ML) approaches. The contributions of this work can be summarized as follows:

- We are investigating the suitability of the RPCA approach on air-ultrasound based defect detection for (near) real-time applications.
- We cast air-ultrasound based defect detection as a low-rank plus sparse recovery problem.
- We compare our model-based RPCA approach with data-driven ML approaches like support vector machines (SVM) [7], k-nearest neighbors (k-NN) [8], deep learning (DL) [9] and gradient boosting trees (GBT) [10].
- Our results show that the RPCA approach is more robust since it has a smaller standard deviation of the defect

detection rates for the same amount of training data compared with data-driven ML approaches. This shows that the proposed method is better at classifying variations in the data, even if they did not appear in the training set. In addition to that, based on our results, our approach performs better than the ML approaches for a small training data set. This is important for the detection of defects of different production lines without having a time-consuming training process.

II. System Overview

This section is organized as follows. In the first subsection II-A, the measurement setup is presented. The following subsection describes the underlying system model. Based on the system model, synthetic data is used to generate a larger data set. The generation of the synthetic data is presented in subsection II-C.

A. Measurement Setup

In this work, an ultrasonic measurement setup as shown in Fig. 1 (a) is utilized. The measurement setup consists of a transmitter (T_X) and a receiver transducer (R_X) of type CF200 from SONOTEC GmbH [11], [12]. Two types of defects were utilized, foam glued on the samples (approx. 1 mm thickness) and drilled holes on the samples' surface. During the measurement, the transducers are moved along a track beside the tested sample. For each step of the track, measurements are recorded while the sample is rotated 360 degrees. To obtain these measurements, a rectangular input signal with 9 volts amplitude is used. Regarding the received signal, the time required for the signal to travel from T_X to R_X is called time-of-flight (TOF, τ, (Fig. 2 Part 1)).
In the following, the structure of the received signal (RS) is analyzed in more detail. As can be seen in Fig. 2, the received signal is divided into three parts. Besides the TOF, the maximum of the first signal wave and the signal trace after the first signal wave are shown in Fig. 2 RS, Part 2 and Part 3. The RS Part 2 corresponds to the line-of-sight. The RS Part 3 consists of many influences like multipath, mode conversion and other influences of the ultrasound channel. The main difference between the received signals through air, defect-free samples, and defective samples is the TOF and the resulting RS Part 2. This is due to the speed of ultrasound

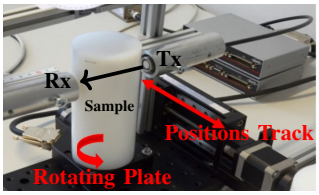

(a) Measurement setup with the transmitter (T_X) and the receiver (R_X) transducer.

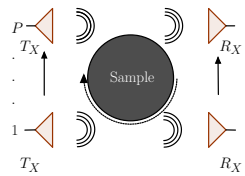

(b) Sketch of the used measurement setup with shown ultrasound waves and a sample.

Fig. 1: Ultrasound measurement setup photograph and schematic. The sample is placed on the rotating plate.

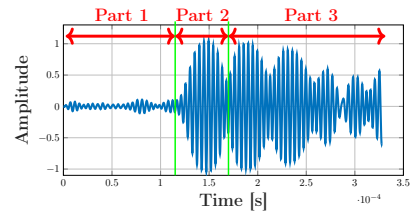

Fig. 2: Separation of the received signal (RS). Part 1: The time-of-flight. Part 2: The maximum of the first signal wave. Part 3: The signal trace after the first signal wave.

in different media, which causes this behavior. For example, air (330 m/s [13]) has a lower ultrasonic speed than a defect-free sample (polyethylene (PE): 2000 m/s [13]). The signal traversing through a defect-free sample reaches the receiver earlier since ultrasound has a higher speed through solids. The received signal is weaker through a sample with foam due to the higher attenuation. Additionally, it reaches the receiver with a larger delay. The TOF differences and the influence of differing acoustic impedance by traversing through different media are used to detect defective samples.

B. System Model

A simplified system model of the measurement setup is established based on the following assumptions and simplifications. For instance, only the line-of-sight is considered over a distance d, and the transducers are assumed to be circular plane pistons with diameter D [14]. For this reason, impairments by the propagation through the ultrasound channel to the receiver such as mode conversion, reflections, and interference of multi-path propagation will be neglected and dumped into the additive noise. With these assumptions, the received signal at timestamp t, position p (where $1 \leq p \leq P$), and q-th angle position (where $1 \leq q \leq Q$), $y_{p,q}(t)$, is given as

$$y_{p,q}(t) = h_{p,q}(t) * x(t) + n(t). \tag{1}$$

Here, the $x(t)$ is the input signal, $h_{p,q}(t)$ is the system response of the ultrasonic channel including the transducers at position p corresponding to the q-th angle position, and $n(t)$ is the receiver noise. In eq. (1), the $*$ represents convolution operation. As shown in Fig. 1 (b), the investigated sample was rotated to record a set of received signals $y_{p,q}(t)$. Here, Q is the number of rotating angle positions corresponding to 360 degrees and P is the total number of positions alongside the positions track. Let the matrix $\mathbf{Y}_p \in \mathbb{R}^{T \times Q}$ be the set of received signals at position p alongside the positions track. Here, T is the number of timestamps. Also, let $\mathbf{Y}_p^i$, $i = 1, 2, 3$, be the component of $\mathbf{Y}_p$ which corresponds to part i of the received signal as shown in Fig. 2.

C. Synthetic Data

It is challenging to generate a large data set based on the measurement data only as the measurements are time-consuming. Therefore, numerical simulations are used to generate a large synthetic data set. As the frequency response of

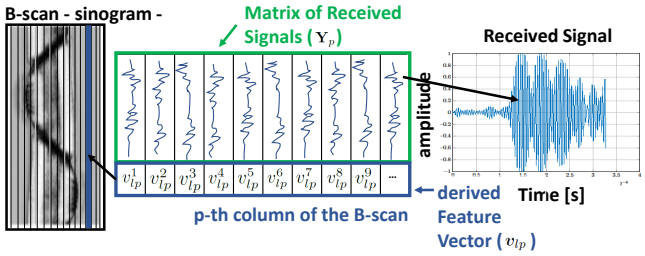

Fig. 3: Sketch of ultrasonic image type sinogram (B-scan). Vector $\boldsymbol{v}_{lp}$ contains the maxima of RS Part 2 of the received signals, which are represented by $v_{lp}^1, \ldots, v_{lp}^Q$. The p-th column of the B-scan is the vector $\boldsymbol{v}_{lp}$.

the input and received signal are known, the system response and thus the frequency response of $h_{p,q}(t)$ $(H_{p,q}(f))$ can be estimated using the Fourier transform of the input signal $(X(f))$ and received signal $(Y_{p,q}(f))$. The analysis of the synthetic data shows highly similar behavior to the measured data. Thus, the synthetic data is used to enlarge the data set.

III. Examination Methods

In this section, the proposed RPCA approach for defect detection is presented. Furthermore, four state-of-the-art ML algorithms are used as a comparison to the RPCA approach. The data used in this investigation are obtained using the measurement setup introduced in II-A and the simulations introduced in II-C. The investigated materials are polyethylene (PE) and Teflon (PTFE) with diameters of $30 - 80$ mm. In air-coupled ultrasound, the inner structures of the object examined can be shown using the sinogram (B-scan) images [15]. Therefore, they are utilized for defect detection using the RPCA approach. The received signal sets of all positions $(\mathbf{Y}_p \ \forall \ p \ \in \{1, .., P\})$ are used to generate the B-scan. This works as follows. Let the B-scan be $\boldsymbol{B} \in \mathbb{R}^{P \times Q}$. In order to generate the B-scan, $P \times Q$ measurements are required. For this, the maximum of each column of the matrix $\mathbf{Y}_p^2$ (maximum of RS Part 2) was used. Let this vector which contains Q number of maxima be given by $\boldsymbol{v}_{lp} \in \mathbb{R}^{Q \times 1}$, with $\boldsymbol{v}_{lp} = [v_{lp}^1, \ldots, v_{lp}^Q]$, for the position p. Now, the B-scan is given by $[\boldsymbol{v}_{l1} \cdots \boldsymbol{v}_{lp} \cdots \boldsymbol{v}_{lP}]^T$ as shown in Fig. 3. In the following, the RPCA approach and ML algorithms are described.

A. Robust principle component analysis

Here, the decomposition of the signaling responses of the defects and the sample from the B-scan $\boldsymbol{B}$ is discussed. An important observation is that the sample response has a low-rank property (i.e., few linearly independent column vectors in the matrix). Further, the defects (foam/drilled holes) response is sparse in nature (few nonzero entries in the matrix). Thus, to identify defects, the rank and sparse properties are utilized. Let the responses of the defects (foam) and the sample be $\boldsymbol{S}, \boldsymbol{L} \ \in \mathbb{R}^{P \times Q}$, respectively. This leads to $\boldsymbol{B} = \boldsymbol{S} + \boldsymbol{L}$. Now, the estimation of $\boldsymbol{S}$ and $\boldsymbol{L}$ can be formulated as an optimization problem, as given below [5], [16]. Here, main objective is to estimate the $\boldsymbol{S}$ and $\boldsymbol{L}$ from $\boldsymbol{B}$.

$$\begin{aligned} \left\{\hat{\boldsymbol{L}}, \hat{\boldsymbol{S}}\right\} &= \min_{\boldsymbol{L},\ \boldsymbol{S}} \operatorname{rank}(\boldsymbol{L}) + \ \lambda_o \parallel \boldsymbol{S} \parallel_0, \\ &\text{s.t. } \|\boldsymbol{B} - \boldsymbol{L} - \boldsymbol{S}\|_F^2 \ \leq \ \epsilon. \end{aligned} \tag{2}$$

Here, rank $(\cdot)$ is the rank of a matrix and it is defined as the maximal number of linearly independent columns of the matrix. The regularization parameter is λ_o and error bound is ϵ, which is a very small positive value. The ℓ^0-norm of a matrix (number of nonzero elements in the matrix) is given as $\|\cdot\|_0$. The term $\|\cdot\|_F$ in eq. (2) is the Frobenius norm. Note that the optimization problem in (2) is non-convex and difficult to solve exactly [17], [18]. Therefore, the nuclear norm (or sum of singular values of the matrix) is used as a convex approximation of the rank. Further, the ℓ^1-norm is used as the convex approximation of the ℓ^0-norm. There are many ways to solve the problem given in eq. (2) [5], [19]. Here, the iterative thresholding approach is utilized due to its computational efficiency. For classification using the RPCA approach, to identify defective samples, the following hypothesis is used

$$\begin{aligned} &\text{No defects } H_0 : \parallel \boldsymbol{S} \parallel_2^2 \leq \delta, \\ &\text{Defects are present } H_1 : \parallel \boldsymbol{S} \parallel_2^2 > \delta. \end{aligned} \tag{3}$$

Here δ is a threshold used to classify defective samples. To obtain δ, training data consisting of defect-free and defective samples are used. Next, based on the eq. (3) the defective and defect-free samples are classified.

B. Machine Learning Approaches

In order to compare the results of the RPCA approach with alternative approaches, four state-of-the-art ML algorithms are employed. Three of these approaches are used for feature-based classification, whereas the deep learning approach is used for image-based classification. The data set used to train and test these algorithms consist of both measurement and synthetic data.

1) Approaches for Feature-Based Classification: Eight features are extracted from the received signals to train and test the ML algorithms, among them the maximum of the first signal wave (maximum of RS Part 2), pulse duration, and the intensity of the the received signal. The training is performed in a supervised manner to distinguish between defective and defect-free samples. In [20], the gradient boosting trees show the best total average classification accuracy compared to eleven state-of-the-art classification algorithms followed by SVM. For this reason, in this work, the two basic ML approaches, k-NN [8], [20], and SVM [7], [20] are applied besides the newer and more efficient GBT [10], [20].

2) Approach for Image-Based Classification: For image-based classification, deep learning is applied as a newer approach besides the GBT. Images of defective and defect-free B-scans are used as input data of the deep learning algorithm. The deep learning model was pre-trained on a large image dataset (i.e., ImageNet). The pre-trained network used in this

Training data portion [%]	k-NN	SVM	GBT	DL	RPCA
100 %	98.53 % ± 0.00	95.29 % ± 0.40	98.82 % ± 0.40	99.41% ± 0.62	98.09 % ± 0.40
75 %	98.53 % ± 0.52	95.15 % ± 1.52	98.53 % ± 0.74	97.06 % ± 4.96	98.09 % ± 0.62
50 %	98.38 % ± 0.33	89.85 % ± 6.56	98.82 % ± 0.66	98.68 % ± 1.09	97.79 % ± 0.52
25 %	97.21 % ± 1.90	92.50 % ± 3.83	98.82 % ± 1.12	96.32 % ± 2.44	97.80 % ± 0.73
10 %	86.47 % ± 5.24	88.52 % ± 2.47	95.00 % ± 2.72	79.56 % ± 6.03	97.94 % ± 0.62
5 %	**74.85 % ± 9.48**	**86.47 % ± 3.98**	**88.82 % ± 1.21**	**73.82 % ± 11.68**	**94.41 % ± 0.39**

TABLE I: Five-fold cross validation results comparison of k-NN, SVM, GBT, DL and the RPCA approaches.

work is SqueezeNet-v1.1 [9]. With transfer learning [21], it was adapted to solve the defect detection in this work. The convolutional layers of the network extract the classification features. The last layer and the final classification layer can be used to detect defective samples. The two layers contain information of combining the features of the network into class probabilities. These two layers have to be replaced by new layers adapted to the new data set to retrain the network.

IV. Results

In this section, the results are presented. First, the result of the RPCA approach is shown and then compared with the results of the ML methods.

A. Robust Principle Component Analysis Approach Result

In this subsection, the result of the RPCA approach is discussed. Fig. 4 shows a PTFE sample decomposition with a 50 mm diameter by the RPCA approach. Here, Fig. 4 (a) shows a B-scan of the 50 mm sample. The reconstructed total response ($\boldsymbol{L}+\boldsymbol{S}$) is shown in Fig. 4 (b). The sparse component (defect/foam) and the low-rank segment (i.e., sample), which are decomposed by the RPCA approach, are shown in Fig. 4 (c) and Fig. 4 (d). Based on the results given in Fig. 4 (d), it is observed that the RPCA approach can successfully identify the defect (foam) of the PTFE 50 mm sample from the B-scan given in 4 (a). In general, defect detection with B-scans are based on the visual inspection. Thus, to have defect detection without visual inspection, the hypothesis given in eq. (3) is used. Fig. 5 shows the process of determining the threshold

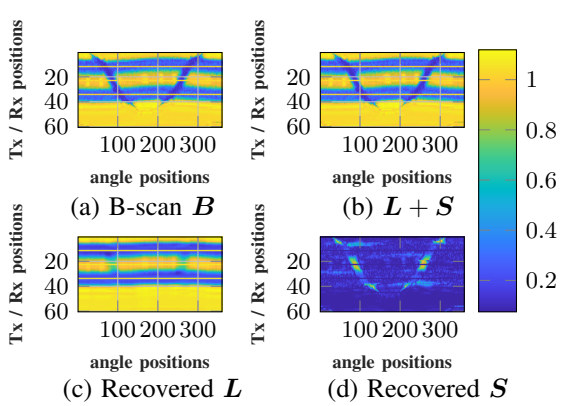

Fig. 4: Decomposition of the B-scan of a 50 mm sample by RPCA approach.

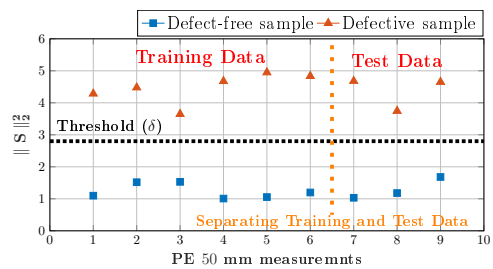

Fig. 5: The threshold (black dotted line) is used to classify the test data as defect-free and defective.

(δ) using the training data. Here, δ is calculated based on the training data as given in

$$\delta = \frac{1}{2}\left(\max\left(\|\boldsymbol{S}_d\|_2^2\right) - \min\left(\|\boldsymbol{S}_{df}\|_2^2\right)\right), \tag{4}$$

where $\boldsymbol{S}_{df}$ and $\boldsymbol{S}_d$ are the sparse components of the RPCA decomposition of the defect free and defective training data set, respectively. Afterwards, the obtained threshold is used for the classification (i.e., defect detection) of the test data.

B. Comparison of the Machine Learning and the Robust Principle Component Analysis Approach

In this subsection, a comparison of the ML approaches with the RPCA approach is presented. For classification purposes, the data was split into training and testing 80 % to 20 %, respectively. A data set, with 680 samples, was used to train and test the ML and RPCA approaches. Here, a hybrid of measured and synthetic data was used to generate the data, where the training and testing data contained 544 and 136 data samples. The data consists of 320 measured and 360 simulated samples. Note that, the data set contains equal percentages of defect free and defective samples. In Table I, the defect detection rates of the ML methods and the RPCA approach and their standard deviation of a five-fold cross validation are compared.

Applying the five-fold cross validation, the mean of the detection rates ($\overline{DR}$) is derived by averaging the runs. The standard deviation (σ_{DR}) is a measure for the variation of the density of probability around $\overline{DR}$ [22], [23]. Therefore, a lower standard deviation means a better result. As shown in the first row of Table I, using 100 % of the training data, the RPCA approach achieves 98.09 % as $\overline{DR}$. This is a comparable result the state-of-the-art ML methods k-NN (98.53 %), SVM (95.29 %), GBT (98.82 %) and DL (99.41 %) achieved.

Reducing the training data step by step, the advantage of RPCA approach becomes more evident. Using 25 % of the training data, the $\overline{DR}$ is still comparable, but the σ_{DR} of the RPCA approach is for the first time lower than all four state-of-the-art ML methods. As the last step, only 5 % of the training data was used. The $\overline{DR}$ of the RPCA approach decreases to 94.41 % with a small σ_{DR} of ± 0.39. In contrast, the $\overline{DR}$ of the ML methods k-NN (74.85 %), SVM (86.47 %), GBT (88.82 %), and DL (73.82 %) decreases stronger for 5 % of the training data set . In the comparison of defect detection rates using the whole training data to the 5 % of the training data, GBT and DL have decreased by approx. 10 % and approx. 20 %, respectively. In contrast, RPCA has only decreased about approx. 4 %.

Moreover, the σ_{DR} of the ML algorithms increases as training data decreases. Especially DL (± 11.68) has a very high σ_{DR} compared to the RPCA approach (± 0.39). The lower σ_{DR} is an essential advantage of the RPCA approach compared to the ML algorithms. This indicate that, the threshold δ can be learned using a few samples in the RPCA approach. Thus, the RPCA approach can be retrained quickly to detect defects in different production lines without having a time-consuming training process. In the comparison, the ML approaches rely on features or images and need a larger training data set to obtain a lower σ_{DR}. Thus, variations of data unseen in the training phase are wrongly classified by the ML algorithms. Achieving high and stable results with small training data sets is an important step to be able to operate near real-time.

V. Conclusion

In this paper, the RPCA approach is compared to the state-of-the-art ML approaches for defect detection by considering various training data sizes. The investigations were performed on an air-coupled ultrasound measurement setup. A hybrid data set of measured and synthetic data was used for classification. The GBT (98.82 %) and DL (99.41 %) outperform all other approaches using 100 % of the training data (680 samples). However, using only 5 % of the training data (34 samples), the mean of detection rates ($\overline{DR}$) of the RPCA approach reaches 94.0 %, which is the best and more stable compared to the detection rates of the ML approaches k-NN (74.85 %), SVM (86.47 %), GBT (88.82 %), and DL (73.82 %). Thus, the $\overline{DR}$ of DL decreases significantly from 99.41 % to 73.82 % as the training data size decreases from 100 % to 5 %. Further, the standard deviation of the detection rates of ML increases significantly compared to the RPCA approach as training data size decreases from 100 % to 5 %. The results showed that the proposed RPCA approach is suitable to operate near real-time using a small training data set. This advantage is important for detecting defects of different production lines without having a time-consuming training process.

Acknowledgment

The authors would like to thank SONOTEC GmbH for providing the transducers of the measurement system. The research project was funded by the Federal Ministry of Economics and Energy (BMWi) via the Arbeitsgemeinschaft industrieller Forschungsvereinigungen (AiF) e. V. on the basis of a resolution of the German Bundestag as part of the programme for the Förderung der industriellen Gemeinschaftsforschung (IGF No. 20345 N).

References

[1] A. Hanida, K. Norazlin, S. Noraidah, and M. Hairulliza, "Statistical process control in plastic packaging manufacturing: A case study," *Int. Conf. on Electr. Eng. and Informat.*, vol. 1, pp. 199–203, 2009.

[2] D. Chimenti, "Review of air-coupled ultrasonic materials characterization," *Ultrasonics*, vol. 54, no. 7, pp. 1804–1816, 2014.

[3] W. Hillger, R. Oster, J. Schuller, R. Stößel , S. Lang, J. Bosse, B. Thaler, D. Ilse, and L. Bühling, "Automated air-coupled ultrasonic technique for the inspection of the ec145 tail boom," *4th Int. Symposium on NDT in Aerospace*, pp. 1–7, 2012.

[4] W. Cobb and J. Johnson, "Ultrasonic monitoring of materials during extrusion manufacture," *IEEE Ultrasonics Symposium. Proc. An Int. Symposium*, 2001.

[5] E. J. Candès, X. Li, Y. Ma, and J. Wright, "Robust principal component analysis?," *Journal of the ACM (JACM)*, vol. 58, no. 3, pp. 1–37, 2011.

[6] J. Wang, Q. Li, J. Gan, H. Yu, and X. Yang, "Surface defect detection via entity sparsity pursuit with intrinsic priors," *IEEE Trans. Ind. Informat.*, vol. 16, no. 1, pp. 141–150, 2020.

[7] C. Cortes and V. Vapnik, "Support-vector networks," *Machine Learning*, vol. 20, pp. 273–297, 1995.

[8] T. Cover and P. Hart, "Nearest neighbor pattern classification," *IEEE Trans. Inf. Theory*, vol. 13, pp. 21–27, 1967.

[9] F. N. Iandola, S. Han, M. W. Moskewicz, K. Ashraf, W. J. Dally, and K. Keutzer, "Squeezenet: Alexnet-level accuracy with 50x fewer parameters and < 0.5 MB model size," *arXiv preprint arXiv:1602.07360*, 2016.

[10] Jerome H Friedman, "Greedy function approximation: a gradient boosting machine," *Annals of statistics*, pp. 1189–1232, 2001.

[11] *Non-contact probes, SONOTEC GmbH*, Available at https://www.sonotec.eu/products/non-destructive-testing/sonoscan-probes/non-contact-probes/.

[12] *Technical Data Sheet: Overview air-coupled ultrasonic probes SONOSCAN CF*, Available at http://www.andesb.com/assets/td_sonoscan_cf_overview_engl_rev_1.1_2016-02-11.pdf.

[13] P. Kinahan, "Physical aspects of medical imaging - lecture 6 ultrasound," 2006.

[14] G. Mazurek, "Basic channel parameters of ultrasound transmission in air," *22nd Int. Microwave and Radar Conf.*, pp. 607–609, 2018.

[15] M. Schwarz, N. Garzorz-Stark, K. Eyerich, J. Aguirre, and V. Ntziachristos, "Motion correction in optoacoustic mesoscopy," *Scientific reports*, vol. 7, no. 1, pp. 1–9, 2017.

[16] J. Wright, A. Ganesh, S. Rao, Y. Peng, and Y. Ma, "Robust principal component analysis: Exact recovery of corrupted low-rank matrices via convex optimization," *Advances in Neural Information Processing Systems*, 2009.

[17] B. Natarajan, "Sparse approximate solutions to linear systems," *SIAM journal on computing*, vol. 24, no. 2, pp. 227–234, 1995.

[18] B. Recht, M. Fazel, and P. Parrilo, "Guaranteed minimum-rank solutions of linear matrix equations via nuclear norm minimization," *SIAM review*, vol. 52, no. 3, pp. 471–501, 2010.

[19] Z. Lin, M. Chen, and Y. Ma, "The augmented lagrange multiplier method for exact recovery of corrupted low-rank matrices," *arXiv:1009.5055*, 2010.

[20] C. Zhang, C. Liu, X. Zhang, and G. Almpanidis, "An up-to-date comparison of state-of-the-art classification algorithms," *Expert Systems with Applications*, vol. 82, pp. 128–150, 2017.

[21] R. Ribani and M. Marengoni, "A survey of transfer learning for convolutional neural networks," pp. 47–57, 2019.

[22] A. Bhusari, N. Gupta, T. Kambli, and S. Kulkami, "Comparison of SVM and kNN classifiers for palm movements using semg signals with different features," *3rd Int. Conf. on Comput. Methodologies and Commun.*, pp. 881–885, 2019.

[23] R. Kohavi, "A study of cross-validation and bootstrap for accuracy estimation and model selection," *Proc. of the 14th Int. Joint Conf. on Artificial Intell.*, p. 1137–1143, 1995.